SEMARAK ILMU PUBLISHING

CFD Letters

Journal homepage:
https://semarakilmu.com.my/journals/index.php/CFD_Letters/index
ISSN: 2180-1363

Radiative Heat Source Fluid Flow of MHD Casson Nanofluid over A Non-Linear Inclined Surface with Soret and Dufour Effects

P. Raja Sekhar[1,2], S. Sreedhar[1,*], S. Mohammed Ibrahim[3], P. Vijaya Kumar[1]

[1] Department of Mathematics, GITAM School of Science, GITAM (Deemed to be University), Visakhapatnam, Andhra Pradesh- 530045, India
[2] Department of FED, NRI IT, Agiripalli, Pothavarappadu (v), Eluru district, Andhra Pradesh - 521212,India
[3] Department of Engineering Mathematics, College of Engineering, Koneru Lakshmaiah Education Foundation, Vaddeswaram, Andhra Pradesh, 522302, India

ARTICLE INFO

Article history:
Received 19 January 2023
Received in revised form 18 February 2023
Accepted 15 March 2023
Available online 1 July 2023

Keywords:
Casson nanofluid; inclination surface; Soret; Dufour; heat source; HAM

ABSTRACT

In this article, the impact of MHD Casson Nanofluid boundary layer flow, over an inclined extending surface with thermal radiation, heat source/sink, Soret and Dufour, is scrutinized. The model used in this study is based on the Buongiorno model of the thermal efficiencies of the fluid flows in the presence of Brownian motion and thermophoresis properties. The non-linear problem for Casson Nanofluid flow over an inclined channel is modeled to gain knowledge on the heat and mass exchange phenomenon, by considering important flow parameters of the intensified boundary layer. The governing non-linear partial differential equations are changed to ordinary differential equations and are afterward illustrated numerically by the homotopy analysis method (HAM). Numerical and graphical results are also presented in tables and graphs. It has been noticed that increasing the inclination parameter reduces the amount of friction experienced by the surface, but it has the opposite effect on the Nusselt number and the Sherwood number. In the concentration field, the inclination parameter reveals a decreasing trend, in contrast to the chemical reaction rate parameter, which reveals an increasing trend in the opposite direction. Likewise, the present results are noticed to be in an excellent agreement with those offered previously by other authors. Finally, some of the physical parameters in this study, which can serve as improvement factors for heat mass transfer and thermophysical characteristics, make nanofluids premium candidates for important future engineering applications.

1. Introduction

In recent times, nanofluid has accomplished an incredible position among scientists because of its dynamic thermal performance and notable potential in the number of heat transfers without any pressure drops. Nanofluid is a formula of various nanoparticles, containing $Al_2 O_3$, Cu, CuO, in a base liquid, for example, oil, water, ethylene glycol, and so forth. It is investigated through examination that the thermal conductivity of base fluid is usually not exactly the same as the nanofluid, Choi and Eastman [1]. Nanofluid is used as a working fluid (base fluid) due to its high thermal conductivity.

* *Corresponding author.*
E-mail address: ssreedhar153@gmail.com (S. Sreedhar)

https://doi.org/10.37934/cfdl.15.7.4260

Buongiorno [2] examined the causes that perform a key job in the advancement of nanofluid's thermal conductivity. He perceived that the Brownian movement and thermophoresis effects in conventional fluid play an important role to enhance the thermal conductivity of the fluid.

According to Eastman *et al.,* [3], the thermal conductivity of nanofluids based on ethylene glycol and incorporating copper nanoparticles was improved. Qasim *et al.,* [4] studied the combined effects of heat and mass transfer in nanofluid thin film over an unsteady stretching sheet using Buongiorno's model. Flow of a power-law fluid film on un unsteady stretching surface was addressed by Andersson *et al.,* [5]. The steady flow of nanofluid on stretching sheet was examined by Khan and Pop [6] Over the past few years, numerous researchers have examined the various fluid flow and heat transfer behaviours of nanofluids [7-9] and noticed that they can achieve improved heat transfer coefficients.

According to the viscosity rule, fluids are divided into two categories: Newtonian fluids and non-Newtonian fluids. Non-Newtonian fluids are used widely in production and engineering, which has stimulated research in this area. The most significant non-Newtonian fluids are Eyring-Powell fluid, micropolar fluid, Walters-B fluid, and Casson fluid. It is challenging to capture all those properties of various non-Newtonian fluids in a single constitutive equation because of the nonlinearity between the stress and the rate of strain for non-Newtonian fluids. This has drawn academics' focus to the study of non-Newtonian fluids' flow dynamics. The Casson fluid is one among the Non-Newtonian fluids. A shear-thinning liquid known as Casson fluid is described as having a yield stress below which no flow occurs, an infinite viscosity at zero rate of shear, and zero viscosity at infinite rate of shear by Arab *et al.,* [10]. By taking into account the Soret-Dufour effects, Ali *et al.,* [11] investigated the Casson fluid flow on a slanted sheet. The Casson fluid flow on vertically inclined sheets was researched by Manideep *et al.,* [12]. The influence of chemical reaction on Casson fluid flow on an inclined plate was examined by Shamshuddin *et al.,* [13]. Vijayaragavan and Kavitha [14] investigated the Casson fluid flow over an inclined plate. By taking into account the hall current, Prasad *et al.,* [15] considered the Casson fluid flow across an inclined sheet. The inclined Casson fluid flow on a permeable sheet was researched by Jain and Parmar [16]. By taking into account the inclined angle result, Sailaja *et al.,* [17] examined the Casson fluid flow on a vertical sheet. Rawi *et al.,* [18] extended the Sailaja *et al.,* [17] by considering over an inclined surface. The Casson fluid flow on a vertically inclined sheet was discussed by Raju *et al.,* [19]. Blood flow modelling is better suited to the Casson fluid model [20, 21]. The work of Mahabaleshwar *et al.,* [22-29] on Casson nanofluid, MHD flow micro polar fluid, and the MHD nanofluid through a permeable and also stretching/shrinking surface, a horizontal surface with a radiating effect with mass transpiration, is well-documented.

Thin fluid flow along an inclined plate has become the subject of more and more studies in recent years. This is because it is important in many physical and engineering settings. These studies are needed to help the theory and applications of thin-film technology in many real-world situations make more sense and move forward. Some examples are the movement of synovial fluid, heat exchangers, lubrication, and the electroplating of surfaces.

Kay *et al.,* [30] proposed the ecological model-based on thin film flow analysis over heated inclined plane. In order to solve the spreading thin fluid problem, Alharbi and Naire [31] developed the R-adaptive mesh method, which takes into account the surface tension at the free surface. A numerical analysis of a thin fluid flow with an outflow down an inclined surface was provided in a work by Shuaib *et al.,* [32]. Experimental results of the thin fluid flow behaviour on the inclined plate were presented by Yu and Cheng [33]. Rafique *et al.,* [34] studied the numerical procedure on Casson nanofluid flow over a non-linear inclined surface in presence of Soret and Dufour effects by Keller-Box method. Recently, different scholars investigated the nanofluid flow on different models, as some of them are given in references [35-37].

Many chemical engineering processes use double diffusive flow (heat and mass transfer). Because of temperature and concentration gradients, buoyancy drives the flow of heat and mass. The simultaneous occurrence of mass and heat transfer in a fluid under motion complicates the relationships between the driving potentials and the energy fluxes. The Soret or thermal-diffusion effect is the mass fluxes produced by temperature gradient, whereas the Dufour or diffusion-thermal effect is the energy flux caused by composition gradient. Due to their smaller order of magnitude as presented by Fick's laws, the effects of both Soret and Dufour have historically received little attention. The Soret effect has been used to separate isotopes. According to Alao *et al.,* [38], Soret and Dufour have opposing effects on the velocity, temperature, and concentration boundary layers. On steady MHD convective flow, Omowaye *et al.,* [39] presented the Dufour and Soret effects on convective flow of fluid through a permable medium with temperature dependent viscosity using HAM method. The study came to the conclusion that an increase in the Dufour number decreases the rate of heat transfer and skin friction coefficient. Amanulla *et al.,* [40] developed a model on MHD Prandtl fluid flow past an isothermal permeable sphere with slip conditions. Using Buongiorno's nanofluid model, Ahmed and Rashed [41] investigated MHD natural convection in wavy enclosures filled with a porous medium that generates heat.

To the best of our awareness, very less research has been conducted on Casson nanofluid towards an inclined stretching surface while taking into account thermal radiation, heat source, chemical reaction, Brownian motion, and the effects of Soret and Dufour. This investigation was motivated by Liao's homotopy analysis method, which was applied in that study. The model under consideration is newly developed from Rafique *et al.,* [34] and results obtained from the current study are new. In this work, we found that the Dufour effect reduces the Nusselt and Sherwood number due to Soret impact. A non-linear form of radiative heat exchange also enhances the fluid temperature. In the future, it can be extended on an exponentially inclined stretching surface.

2. Physical and Mathematical Model

Considered here is the continuous flow of a two-dimensional boundary layer of Casson Nano fluid over a non-linear surface that extends at an angle Ω. It is assumed that the extending and free stream velocities are, respectively, $u_w(x) = ax^m$ and $u_\infty(x) = 0$. Where, with "*a*" assumed to be constant, *x* is the coordinate that has been dignified in the direction of the surface that is expanding. We are going to suppose that there is an external transverse magnetic field that is normal to the flow route. It is important to take into account the Brownian motion and the thermophoresis effects. The temperature *T* and *C* the nano particle fraction at the wall adopt the constant values T_w and C_w, whereas the ambient forms for the nanofluid mass and temperature fractions C_∞ and T_∞ are completed as *y* approaches to immensity, as illustrated in Figure 1.

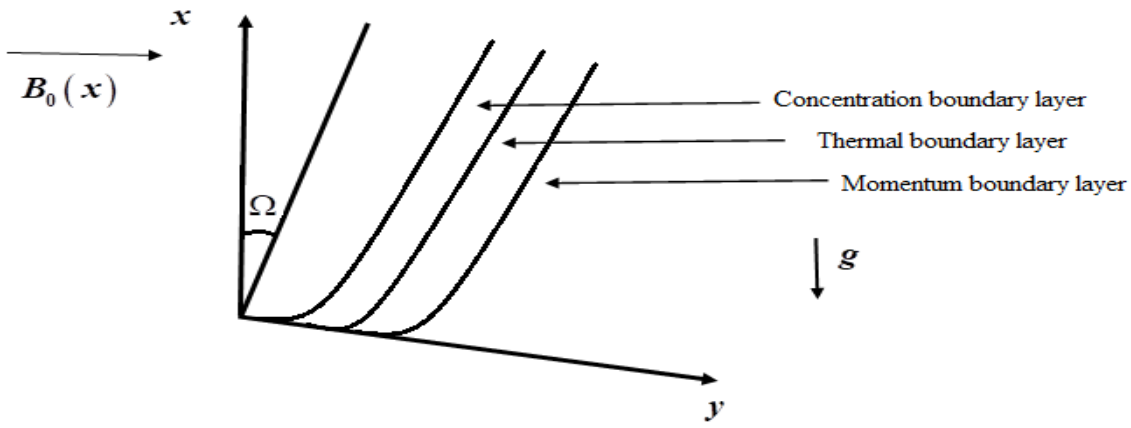

Fig. 1. Geometry of the physical model and the coordinate system

Using these assumptions, the modelled governing equations are defined as follows [6, 34]

$$\frac{\partial u}{\partial x}+\frac{\partial v}{\partial y}=0, \tag{1}$$

$$u\frac{\partial u}{\partial x}+v\frac{\partial u}{\partial y}=\nu\left(1+\frac{1}{\beta}\right)\frac{\partial^2 u}{\partial y^2}+g\left[\beta_t\left(T-T_\infty\right)+\beta_c\left(C-C_\infty\right)\right]\cos\Omega-\frac{\sigma B_0^2(x)u}{\rho}, \tag{2}$$

$$u\frac{\partial T}{\partial x}+v\frac{\partial T}{\partial y}=\alpha\frac{\partial^2 T}{\partial y^2}-\frac{1}{\left(\rho c_p\right)_f}\frac{\partial q_r}{\partial y}+\tau\left[D_B\frac{\partial C}{\partial y}\frac{\partial T}{\partial y}+\frac{D_T}{T_\infty}\left(\frac{\partial T}{\partial y}\right)^2\right]$$
$$+\frac{D_T K_T}{C_s C_p}\frac{\partial^2 C}{\partial y^2}+\frac{Q_0}{\left(\rho c_p\right)_f}(T-T_\infty), \tag{3}$$

$$u\frac{\partial C}{\partial x}+v\frac{\partial C}{\partial y}=D_B\frac{\partial^2 C}{\partial y^2}+\frac{D_T K_T}{T_\infty}\frac{\partial^2 T}{\partial y^2}-Kr\left(C-C_\infty\right), \tag{4}$$

For the sake of this discussion, the Rosseland approximation (for radiation flux) is defined as follows:

$$q_r=-\frac{4\sigma^*}{3k^*}\frac{\partial T^4}{\partial y}. \tag{5}$$

where k^* is the average absorption coefficient, σ^* is the Stefan-Boltzmann constant, and T^4 is a linear function of temperature (the temperature gradient inside the flow). We obtain after filtering out the T^4's higher-order terms in the Taylor series expansion of

$$T^4=4T_\infty^3 T-3T_\infty^4 \tag{6}$$

Then, with the help of Eqs. (6) and (7), we obtain

$$u\frac{\partial T}{\partial x}+v\frac{\partial T}{\partial y}=\left(\alpha+\frac{16\sigma^{*}}{3k^{*}\left(\rho c_{p}\right)_{f}}\right)\frac{\partial^{2}T}{\partial y^{2}}+\tau\left[D_{B}\frac{\partial C}{\partial y}\frac{\partial T}{\partial y}+\frac{D_{T}}{T_{\infty}}\left(\frac{\partial T}{\partial y}\right)^{2}\right]+\frac{D_{T}K_{T}}{C_{s}C_{p}}\frac{\partial^{2}C}{\partial y^{2}}, \tag{7}$$

here u and v are the velocity components in the x and y directions, respectively, g is the acceleration due to gravity, B_0 is the identical magnetic field strength, σ is the electrical conductivity, μ is the viscosity, δ_f is the density of the base fluid, δ_p is the density of the nanoparticle, β is the Casson parameter, β_t is the coefficient of thermal expansion, β_c is the coefficient of concentration expansion, D_B is the Brownian diffusion coefficient and D_T is the thermophoresis diffusion coefficient, k is the thermal conductivity, $\left(\rho c\right)_p$ is the heat nanoparticles capacitance, $\left(\delta c\right)_f$ is the base fluid heat capacitance, $\alpha=\dfrac{k}{\left(\rho C_{p}\right)_{f}}$ is the thermal diffusivity constraint, $\tau=\dfrac{\left(\rho C_{p}\right)_{p}}{\left(\rho C_{p}\right)_{f}}$ is the proportion of the nanoparticle's effective heat capacity to the total heat capacity of the fluid., K_r is the chemical reaction (destructive) constraint.

The subjected boundary conditions are Ref. [34]:

$$\begin{aligned}&u=u_{w}\left(x\right)=ax^{m},v=0,T=T_{w},C=C_{w},aty=0\\&u\to u_{\infty}\left(x\right)=0,v\to 0,T\to T_{\infty},C\to C_{\infty}aty\to\infty,\end{aligned} \tag{8}$$

A reduction is made from the non-linear partial differential equations to the non-linear ordinary differential equations. For that purpose, the stream function $\psi=\psi\left(x,y\right)$ is defined as:

$$u=\frac{\partial\psi}{\partial y},v=-\frac{\partial\psi}{\partial x}, \tag{9}$$

The continuity equations are considered to be satisfied in their entirety when defined.

The other features were measured according to Ref. [34]. The below formulas were applied for simplifying the equations Ref. [34]:

$$\begin{aligned}&\zeta=y\sqrt{\frac{\left(m+1\right)ax^{m-1}}{2v}},\psi=\sqrt{\frac{2vax^{m+1}}{m+1}}f\left(\eta\right),\theta\left(\eta\right)=\frac{T-T_{\infty}}{T_{w}-T_{\infty}}\\&\phi\left(\eta\right)=\frac{C-C_{\infty}}{C_{w}-C_{\infty}},\end{aligned} \tag{10}$$

So, the final form of equations contains three scalars which should be calculated for each node Ref. [34]:

$$\left(1+\frac{1}{\beta}\right)f'''+ff''-\frac{2m}{m+1}f'^{2}+\frac{2}{m+1}(\lambda\theta-\delta\varphi)\cos\Omega-\left(\frac{2M}{m+1}\right)f'=0 \tag{11}$$

$$\left(1+\frac{4}{3}R\right)\theta''+\Pr f\theta'+\Pr Nb\phi'\theta'+\Pr Nt\theta'^{2}+D_f\phi+\frac{2}{m+1}Q\Pr\theta=0, \tag{12}$$

$$\phi''+\Pr Lef\phi'+\frac{Nt}{Nb}\theta''-\frac{2}{m+1}\Pr Le\gamma\phi=0 \tag{13}$$

Where,

$$\lambda=\frac{Gr_x}{\mathrm{Re}},\delta=\frac{Gc}{\mathrm{Re}},M=\frac{\sigma B_0^2(x)}{\rho a},Le=\frac{v}{D_B},\Pr=\frac{v}{\alpha},N_b=\frac{\tau D_B(C_w-C_\infty)}{v},$$
$$N_t=\frac{\tau D_t(T_w-T_\infty)}{vT_\infty},Gr_x=\frac{g\beta_t(T_w-T_\infty)x}{av},\mathrm{Re}=\frac{u_w x}{v},Gc_x=\frac{g\beta_c(C_w-C_\infty)x}{av},$$
$$R=\frac{4\sigma^*T_\infty^3}{\alpha k^*},D_f=\frac{D_TK_T(C_w-C_\infty)}{vC_sC_p(T_w-T_\infty)},Sr=\frac{D_TK_T(T_w-T_\infty)}{vT_\infty(C_w-C_\infty)},\gamma=\frac{K_r}{a(C_w-C_\infty)}$$

In this case, primes indicate the differentiation with respect to ζ, the buoyancy consideration λ, the solutal buoyancy consideration δ, the magnetic parameter, which is referred to as the Hartmann number is *M*, the kinematic viscosity of the liquid v, the Prandtl number Pr, the Lewis number Le, the Brownian motion consideration N_b, the thermophoresis consideration N_t, the radiation consideration *R*, and the chemical reaction consideration γ.

The corresponding boundary conditions are transformed to:

$$\begin{aligned}&f(\zeta)=0,f'(\zeta)=1,\quad\phi(\zeta)=1,\quad\theta(\zeta)=1\quad at\quad\zeta=0,\\&f'(\zeta)\to0,\theta(\zeta)\to0,\phi(\zeta)\to0\ as\quad\zeta\to\infty,\end{aligned} \tag{14}$$

For the sake of this particular problem, the definitions of skin friction, the Sherwood number, and the Nusselt number are as follows:

$$Cf=\frac{\tau_w}{\rho u_w^2\rho_f},\ Nu_x=\frac{xq_w}{k(T_w-T_\infty)},\ Sh_x=\frac{xq_m}{D_B(C_w-C_\infty)}\ ,$$

$$q_w=-k\frac{\partial T}{\partial y},q_m=-D_B\frac{\partial C}{\partial y},\tau_w=\mu\left(1+\frac{1}{\beta}\right)\frac{\partial u}{\partial y}aty=0$$

Expressions such as the dimensionless reduced Nusselt number $-\theta'(0)$, the reduced Sherwood number $-\phi'(0)$, and the skin friction coefficient C_{fx} can be defined as follows:

$$-\theta'(0)=\frac{Nu_x}{\left(1+\frac{4}{3}N\right)\sqrt{\frac{m+1}{2}\mathrm{Re}}},-\phi'(0)=\frac{Sh_x}{\sqrt{\frac{m+1}{2}\mathrm{Re}}},\left(1+\frac{1}{\beta}\right)f''(0)=C_f\sqrt{\frac{2}{m+1}\mathrm{Re}}$$

where, Reynolds number (local) is defined as $\mathrm{Re}_x=\frac{u_w x}{\nu}$.

2.1 HAM

Following is a rundown of the initial guesses and linear operators that must be used in order to obtain the homotopic solutions of Eqs. (11)–(14).

$$f_O(\zeta)=\left(1-e^{-\zeta}\right),$$
$$\theta_O(\zeta)=e^{-\zeta},$$
$$\phi_O(\zeta)=e^{-\zeta}.$$

$$L_I(f)=f'''-f',$$
$$L_{II}(\theta)=\theta''-\theta,$$
$$L_{III}(\varphi)=\varphi''-\varphi,$$

with

$$L_I\left(C_1+C_2e^{\zeta}+C_3e^{-\zeta}\right)=0,$$
$$L_{II}\left(C_4e^{\zeta}+C_5e^{-\zeta}\right)=0,$$
$$L_{III}\left(C_6e^{\zeta}+C_7e^{-\zeta}\right)=0,$$

where c_j ($j=1.0\,\text{to}\,7.0$) are the subjective factors.

In this step, the zeroth-order deformation equations are constructed.

$$(1-\mathrm{P})L_I\left(f(\zeta;\mathrm{P})-f_0(\zeta)\right)=\mathrm{P}\hbar_I N_I\left[f(\zeta;\mathrm{P}),\theta(\zeta;\mathrm{P}),\phi(\zeta;\mathrm{P})\right], \quad (15)$$

$$(1-\mathrm{P})L_{II}\left(\theta(\zeta;\mathrm{P})-\theta_0(\zeta)\right)=\mathrm{P}\hbar_{II} N_{II}\left[f(\zeta;\mathrm{P}),\theta(\zeta;\mathrm{P}),\varphi(\zeta;\mathrm{P})\right], \quad (16)$$

$$(1-\mathrm{P})L_{III}\left(\varphi(\zeta;\mathrm{P})-\varphi_O(\zeta)\right)=\mathrm{P}\hbar_{III} N_{III}\left[f(\zeta;\mathrm{P}),\theta(\zeta;\mathrm{P}),\phi(\zeta;\mathrm{P})\right], \quad (17)$$

conditional on the existence of the boundary conditions

$$\begin{aligned} &f(0;\mathrm{P})=0, && f'(0;\mathrm{P})=1, && f'(\infty;\mathrm{P})=0,\\ &\theta(0;\mathrm{P})=1, && && \theta(\infty;\mathrm{P})=0,\\ &\phi(0;\mathrm{P})=1, && && \phi(\infty;\mathrm{P})=0, \end{aligned} \tag{18}$$

$$\begin{aligned} N_{II}\left[\varphi(\zeta,\mathrm{P}),\theta(\zeta;\mathrm{P}),f(\zeta;\mathrm{P}),\right] &= f(\zeta;\mathrm{P})f''(\zeta;\mathrm{P})+\left(\frac{1}{\beta}+1\right)f'''(\zeta;\mathrm{P})\\ -\frac{(2m)}{1+m}\left(f'(\zeta;\mathrm{P})\right)^2+\frac{2}{1+m}&\left(\lambda\theta(\zeta;\mathrm{P})\cos\Omega-\delta\phi\cos\Omega\right)-\frac{2M}{1+m}f'(\zeta;\mathrm{P}), \end{aligned} \tag{19}$$

$$\begin{aligned} N_{II}\left[\phi(\zeta;\mathrm{P}),\theta(\zeta;\mathrm{P}),f(\zeta;\mathrm{P}),\right] &= \left(f(\zeta;\mathrm{P})\frac{\partial\theta(\zeta;\mathrm{P})}{\partial\zeta}\right)+Nt\left(\frac{\partial\theta(\zeta;\mathrm{P})}{\partial\zeta}\right)^2\\ +Nb\frac{\partial\theta(\zeta;\mathrm{P})}{\partial\zeta}\frac{\partial\phi(\zeta;\mathrm{P})}{\partial\zeta}&+D_f\frac{\partial^2\phi(\zeta;\mathrm{P})}{\partial\zeta^2}+\frac{2}{m+1}Q\theta+\frac{1}{\mathrm{Pr}}\left(1+\frac{4}{3}R\right)\frac{\partial^2\theta(\zeta;\mathrm{P})}{\partial\zeta^2}, \end{aligned} \tag{20}$$

$$\begin{aligned} N_{III}\left[\phi(\zeta;\mathrm{P}),f(\zeta;\mathrm{P}),\theta(\zeta;\mathrm{P})\right] &= \frac{\partial^2\phi(\zeta;\mathrm{P})}{\partial\zeta^2}+Le\,\mathrm{Pr}\left(f(\zeta;\mathrm{P})\frac{\partial\phi(\zeta;\mathrm{P})}{\partial\zeta}-\frac{2}{n+1}\gamma\phi\right)\\ +\mathrm{Pr}\,Le\,Sr\frac{\partial^2\theta(\zeta;\mathrm{P})}{\partial\zeta^2}&, \end{aligned} \tag{21}$$

When the value of P is equal to zero and one, we can get the resultant flow, thermal and volume fraction functions as

$$\begin{aligned} &f(\zeta;0)=f_0(\zeta) && f(\zeta;1)=f(\zeta),\\ &\theta(\zeta;0)=\theta_0(\zeta) && \theta(\zeta;1)=\theta(\zeta),\\ &\phi(\zeta;0)=\phi_0(\zeta) && \phi(\zeta;1)=\phi(\zeta). \end{aligned} \tag{22}$$

When a result, P as the acceleration changes from 0 to 1, the resulting solutions $f(\zeta;\mathrm{P}),\ \theta(\zeta;\mathrm{P})$ and $\phi(\zeta;\mathrm{P})$ of the original nonlinear differential equations might range from initial approximations to perfect solutions.

with the help of series on Taylor's model , we get

$$f(\zeta;\mathrm{P})=f_0(\zeta)+\sum_{N=1}^{\infty}f_N(\zeta)\mathrm{P}^N, \tag{23}$$

$$\theta(\zeta;\mathrm{P})=\theta_0(\zeta)+\sum_{N=1}^{\infty}\theta_N(\zeta)\mathrm{P}^N, \tag{24}$$

$$\varphi(\zeta;\mathrm{P})=\varphi_0(\zeta)+\sum_{N=1}^{\infty}\varphi_N(\zeta)\mathrm{P}^N, \tag{25}$$

Where

$$f_N(\zeta)=\frac{1}{N!}\frac{\partial^N f(\zeta;\mathrm{P})}{\partial \mathrm{P}^N}\bigg|_{p=0},$$
$$\theta_N(\zeta)=\frac{1}{N!}\frac{\partial^N \theta(\zeta;\mathrm{P})}{\partial \mathrm{P}^N}\bigg|_{p=0}, \quad (26)$$
$$\varphi_N(\zeta)=\frac{1}{N!}\frac{\partial^N \varphi(\zeta;\mathrm{P})}{\partial \mathrm{P}^N}\bigg|_{p=0}.$$

It is possible to achieve convergence of the series (22) to (25) by selecting appropriate initial approximations, auxiliary linear operators, and non-zero auxiliary parameters.

$$f(\zeta)=f_0(\zeta)+\sum_{N=1}^{\infty} f_N(\zeta), \quad (27)$$

$$\theta(\zeta)=\theta_0(\zeta)+\sum_{N=1}^{\infty}\theta_N(\zeta), \quad (28)$$

$$\phi(\zeta)=\phi_0(\zeta)+\sum_{N=1}^{\infty}\phi_N(\zeta). \quad (29)$$

N^{th}-order deformation equations are as follows

$$L_1\left(f_N(\zeta)-\chi_N\, f_{N-1}(\zeta)\right)=\hbar_1 R_N^f(\zeta), \quad (30)$$

$$L_2\left(\theta_N(\zeta)-\chi_N\,\theta_{N-1}(\zeta)\right)=\hbar_2 R_N^\theta(\zeta), \quad (31)$$

$$L_3\left(\varphi_N(\zeta)-\chi_N\,\varphi_{N-1}(\zeta)\right)=\hbar_3 R_N^\varphi(\zeta), \quad (32)$$

with the resulting frontier situations

$$\begin{aligned} &f_N(0)=0, \quad f_N'(0)=0, \quad f_N'(\infty)=0,\\ &\theta_N'(0)=0, \quad \theta_N(\infty)=0, \quad (33)\\ &\varphi_N(0)=0, \quad \varphi_N(\infty)=0, \end{aligned}$$

where

$$R_N^f(\zeta)=\left(1+\frac{1}{\beta}\right)f_{N-1}^{'''}+\sum_{j=0}^{N-1}f_{N-1-j}f_j^{''}-\frac{2m}{m+1}\sum_{j=0}^{N-1}f_{N-1-j}^{'}f_j^{'}+\frac{2m}{m+1}(\ \lambda\theta_{N-1}-\delta\ \phi_{N-1})\cos\Omega$$
$$-\frac{2M}{m+1}f_{N-1}^{'}, \tag{34}$$

$$R_N^\theta(\zeta)=\frac{1}{\Pr}\left(1+\frac{4R}{3}\right)\theta_{N-1}^{''}+\sum_{i=0}^{n-1}f_{N-1-j}\theta_j^{'}+Nb\sum_{i=0}^{n-1}\theta'_{N-1-j}\phi_j^{'}$$
$$+Nt\sum_{j=0}^{N-1}\theta'_{N-1-j}\theta_j^{'}-\Pr D_f\phi_{N-1}^{''}+\frac{2}{m+1}\Pr\theta_{N-1}Q, \tag{35}$$

$$R_N^\phi(\zeta)=\phi_{N-1}^{''}+Le\Pr\left(\sum_{j=0}^{N-1}f_{N-1-j}\phi_j^{'}-\gamma\phi_{N-1}\right)+\Pr Sr\ Le\ \theta_{N-1}^{''}, \tag{36}$$

$$\chi_N=\begin{cases}0, & N\le 1,\\ 1, & N>1.\end{cases} \tag{37}$$

2.2 The Solution Converges on the HAM Model

Figure 2 depicts $\hbar$-curves, which can be used to determine appropriate values for certain parameters. The feasible range of the parameters is approximately $[-1.0, 0.0]$, as determined by a careful examination of the diagrammatic depiction. The outcomes converge when $\hbar-0.45$ in the region of ζ. Table 1 is the convergence of adopted approach.

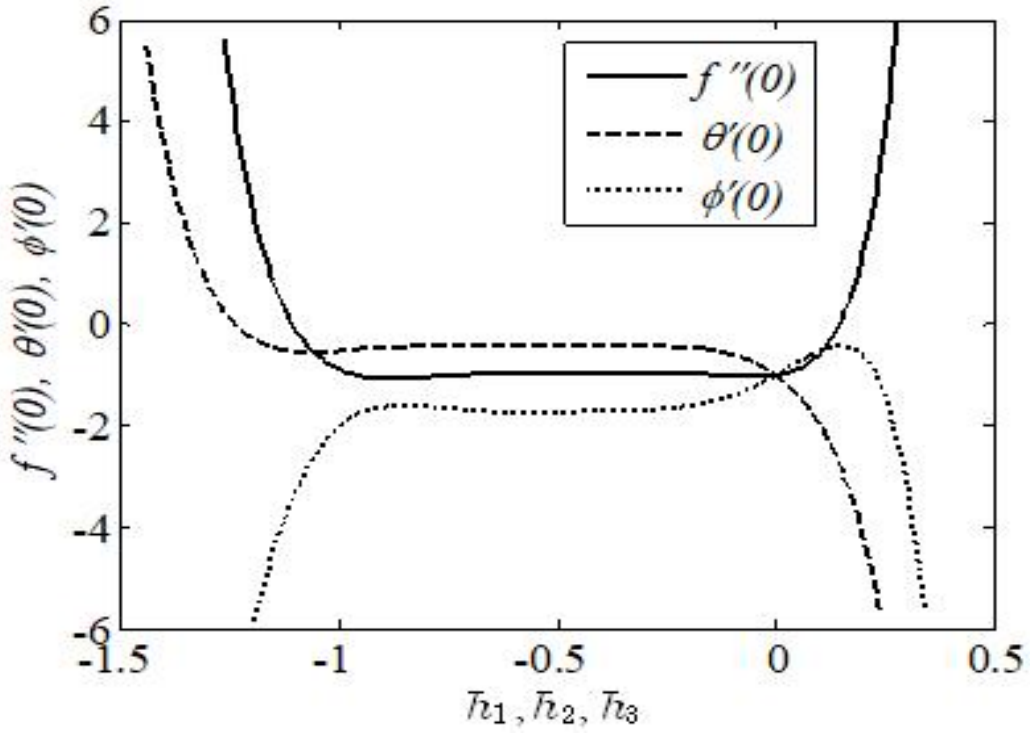

Fig. 2. $\hbar$-curves of $f''(0)$, $\theta'(0)$ and $\phi'(0)$

Table 1
Convergence of solutions to HAM problems across a variety of orders of approximation when
$\beta = 1.0, M = m = 0.5, \lambda = R = Sr = D_f = Q = 0.1, \delta = 0.9, \Pr = Le = 2.0,$
$Nb = Nt = \gamma = 0.2, \Omega = \pi / 4.$

Order	$-f''(0)$	$-\theta'(0)$	$-\phi'(0)$
5	0.976101	0.281246	1.81977
10	0.976165	0.278247	1.820326
15	0.976174	0.277886	1.820271
20	0.976172	0.277842	1.820276
25	0.976172	0.277835	1.820277
30	0.976172	0.277834	1.820277
35	0.976172	0.277834	1.820277
40	0.976172	0.277834	1.820277
45	0.976172	0.277834	1.820277

Table 2
Comparison of $-\theta'(0)$ for different values of Nb and Nt when
$M = R = \lambda = \delta = Sr = D_f = 0, \beta \to \infty, m = 1, \Pr = Le = 10, \Omega = \pi / 2.$

		Rafique et al. [34]		HAM	
Nb	Nt	$-\theta'(0)$	$\phi'(0)$	$-\theta'(0)$	$\phi'(0)$
0.1	0.1	0.9524	2.1294	0.952428	2.129471
0.2	0.2	0.3654	2.5152	0.365436	2.515266
0.3	0.3	0.1355	2.6088	0.135545	2.608814

The Values of $-\theta'(0)$ and $\phi'(0)$ for different ranges of Nb and Nt are determined and compared to formerly existing work in Table 2. The current results are found to be in limiting sense agreement with the preceding results.

3. Results and Discussion

Here, we provide graphical and tabular interpretations of the features of physical variables such velocity, temperature, concentration, skin friction, Nusselt and Sherwood numbers. Some of the figures are generated by varying the value of a parameter within a predetermined range, while others, and are always maintained at the same value such as

$$\beta = 1.0, M = m = 0.5, \lambda = R = Sr = D_f = Q = 0.1, \delta = 0.9, \Pr = Le = 2.0,$$
$$Nb = Nt = \gamma = 0.2, \Omega = \pi / 4.$$

An image of the effect of factor M on velocity profile is portrayed in Figure 3. According to Figure 3, by improving the constraint M, the velocity outline reduces. Due to the magnetic field produces Lorentz force, by slowing down the speed of the liquid.

On the other hand, the velocity profile slows down for large values of the non-linear stretching parameter m, shown in Figure 4. Physically, the momentum boundary layer thickness reduces for

higher values of *m*. The impact of the buoyancy factor λ is shown in Figure 5. It is observed that the velocity profile rises by improving the buoyancy limit. It is due to the fact that buoyancy effect increases the strength of the fluid flow whereby the boundary layer thickness and velocity enhances.

Figure 6 indicates that the velocity outline increases by enhancing the solutal buoyancy factor δ . Physically, the buoyancy parameter reduces the viscous forces whereby the velocity upturns.

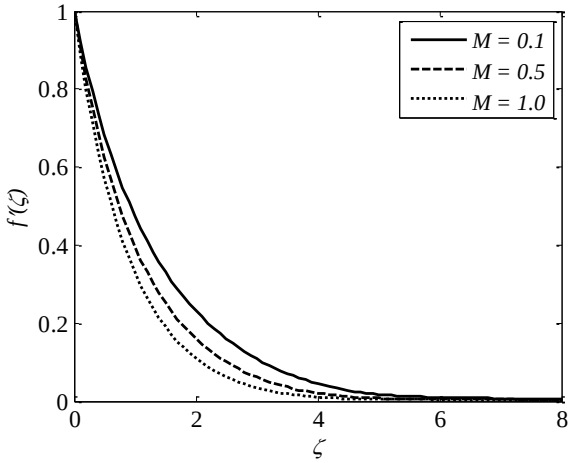

Fig. 3. Impact of M on $f'(\zeta)$

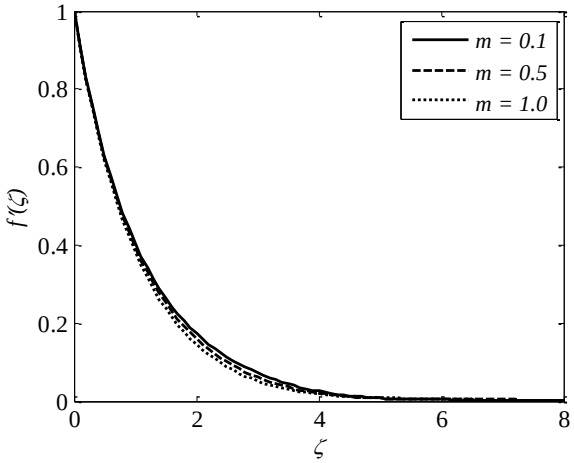

Fig. 4. Impact of m on $f'(\zeta)$

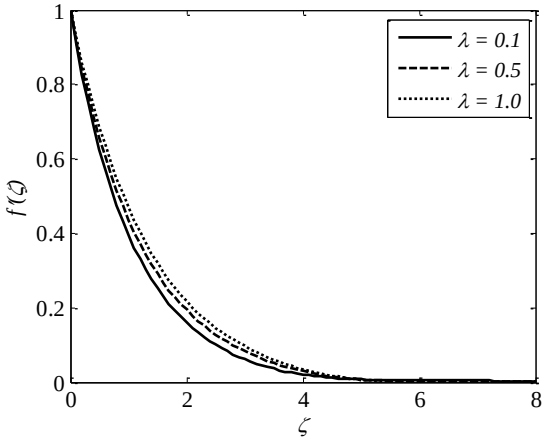

Fig. 5. Impact of λ on $f'(\zeta)$

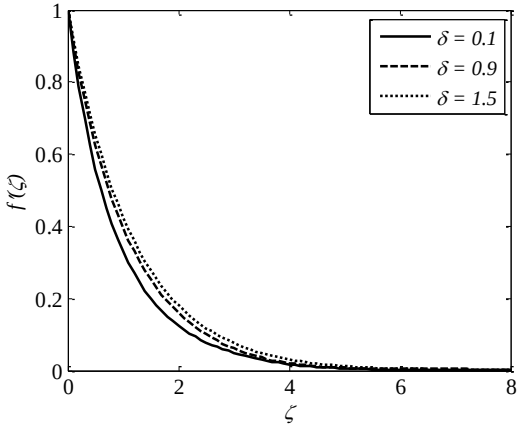

Fig. 6. Impact of δ on $f'(\zeta)$

Figure 7 interprets the significance of inclination factor Ω on the velocity outline. It is perceived in Figure 7 that the velocity outline runs down by enhancing the values of Ω. Moreover, the circumstances indicate that the maximum gravitational force acts on flow in the case of $\Omega = 0$, because in this state the sheet will be vertical. On the other hand, for $\Omega = 90^0$, the sheet will be horizontal which causes the decline in velocity profile as the power of the bouncy forces drop.

The effect of the Casson parameter β on the velocity parameter is presented in Figure 8. It is observed that for large values of the Casson parameter, the velocity profile decreases. The reason behind this behavior is that by increasing the values of the Casson parameter, β increases the fluid viscosity i.e., reducing the yield stress. Therefore, the momentum boundary layer thickness reduces.

Figures 9-10 show the effect of the Brownian motion on the temperature and concentration profiles, respectively. The temperature sketch enlarges on enlarging *Nb*; on the other hand, concentration distribution enlightens a dissimilar style. Physically, the boundary layer heats up due

to the development in the Brownian motion which is inclined to transport nanoparticles from the extending sheet to the motionless liquid. Therefore, the absorption nanoparticle lessens.

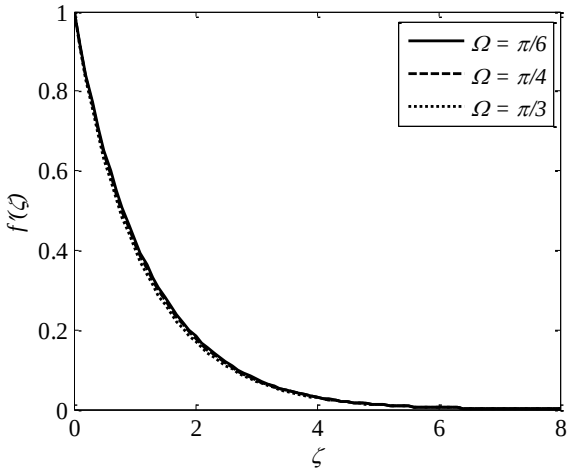

Fig. 7. Impact of Ω on $f'(\zeta)$

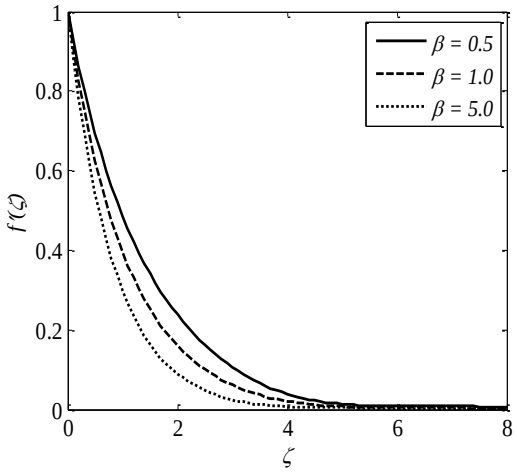

Fig. 8. Impact of β on $f'(\zeta)$

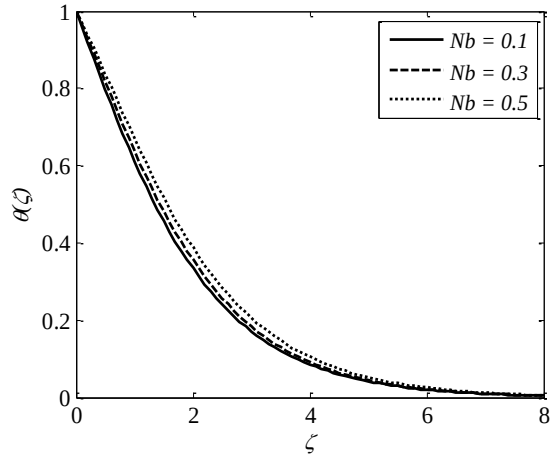

Fig. 9. Impact of Nb on $\theta(\zeta)$

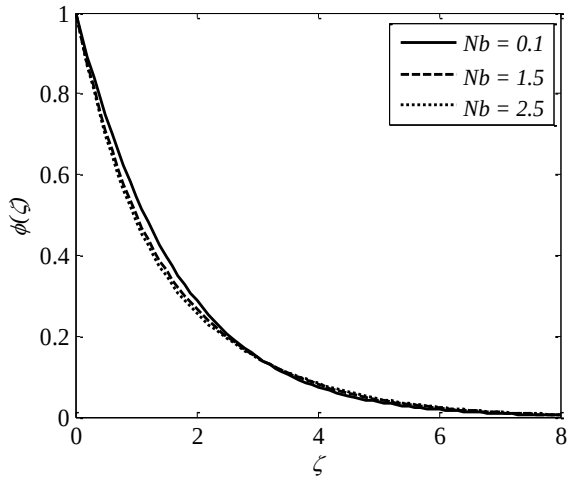

Fig. 10. Impact of Nb on $\phi(\zeta)$

Figures 11-12 present temperature and concentration profiles for altered values of thermophoresis parameters Nt. It is perceived that both temperature and concentration contours upsurge by growing the thermophoresis parameter because thermophoresis causes the small particles to compel away from a warm surface to the cold one.

Figure 13 shows that the temperature profile becomes large for larger values in parameter D_f. This can be justified as an increase in the Dufour parameter, causing an increase in the concentration gradient, resulting in a mass diffusion taking place more rapidly. In this way, the rate of energy transfer related to the particles becomes higher. That is why the temperature profiles enhance. The impact of the Soret number Sr on the concentration profile is observed similar to the impact of the Dufour number on the temperature profile. As parameter Sr increases, the concentration profile increases as displayed in Figure 14.

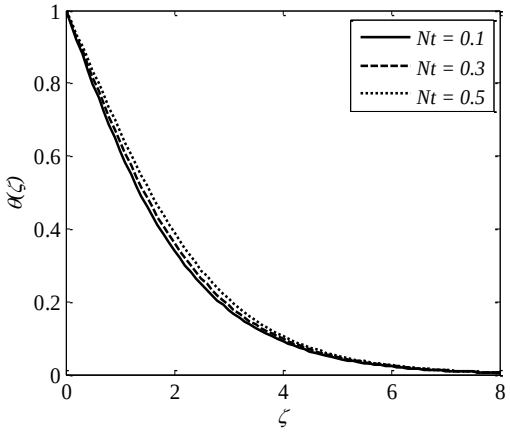

Fig. 11. Impact of Nt on $\theta(\zeta)$

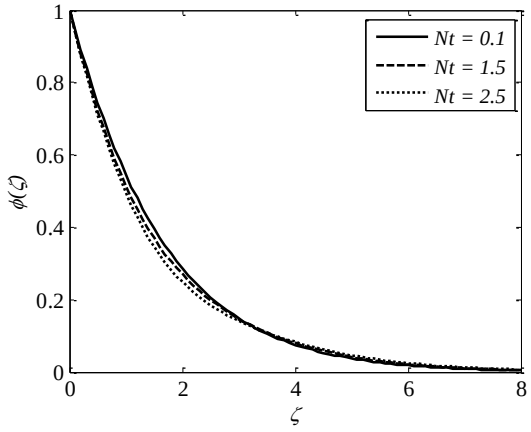

Fig. 12. Impact of Nt on $\phi(\zeta)$.

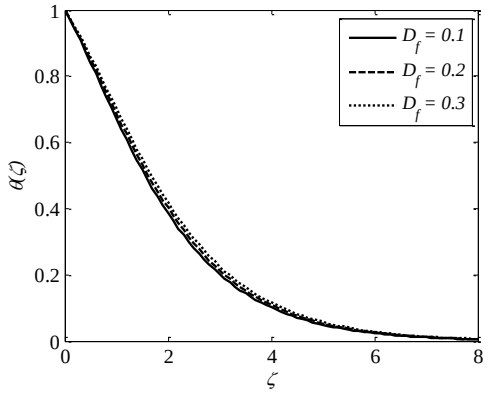

Fig. 13. Impact of D_f on $\theta(\zeta)$

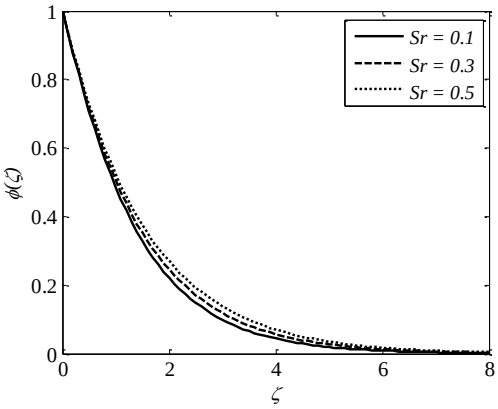

Fig. 14. Impact of Sr on $\phi(\zeta)$

Figure 15 displays the effect of the heat-generating parameter Q on the temperature distribution. As can be observed, increasing the intensity of the heat source ($Q>0$) results in a rise in temperature. This is because to the production of more heat in the thermal boundary layer, which is raising overall temperatures. As demonstrated in Figures 16 and 17, fields of temperature and nanoparticle concentration are plotted against Prandtl number $\Pr$. Both the temperature and the concentration of nanoparticles in the boundary layer are demonstrated to decrease with increasing Prandtl number. Low thermal diffusivity at high Prandtl numbers causes thicker thermal and nanoparticle concentration boundary layers. Figure 18 provides a visual representation of the effect that the Lewis number Le has on the concentration field. As the Lewis number increases, the concentration field drops, resulting in low molecular diffusivity and a narrower boundary layer. Additionally, the weaker molecular diffusivity indicates that the boundary layer is getting thinner. Figure 19 illustrates the impact that a chemical reaction has on the concentration profile that is produced as a result. As the value of the chemical parameter goes up, one notices that the concentration profile is going in the opposite direction, dropping. This occurs as a result of the presence of a corrosive chemical, which causes the thickness of the solutal boundary layer to decrease while simultaneously increasing the mass transfer rates.

The radiation parameter estimates the relevance of thermal radiation transmission in comparison to convective heat transfer. Thermal characteristics enhance of radiation parameter increases for nanoparticles tested scenarios studied, as shown in Figure 20. It is observed that thermal radiation has a greater impact on increasing the nanofluid temperature. Physically, strengthening radiative

features stimulate the molecule mobility within the fluid, resulting in heat energy being converted through frequent collisions between nanoparticles.

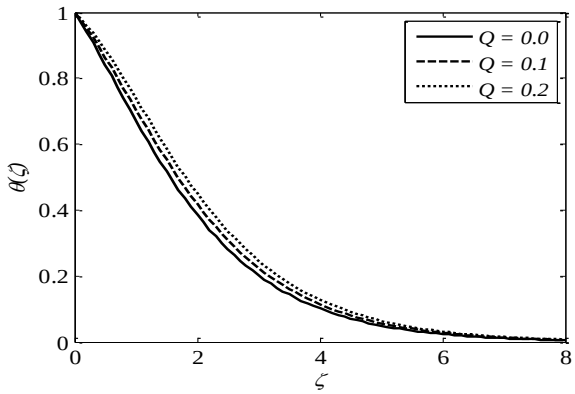

Fig. 15. Impact of Q on $\theta(\zeta)$

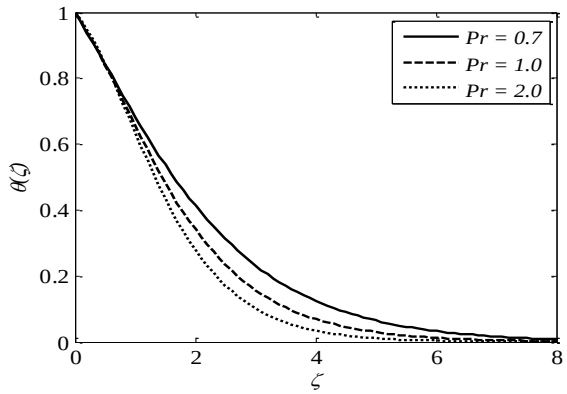

Fig. 16. Impact of $\Pr$ on $\theta(\zeta)$

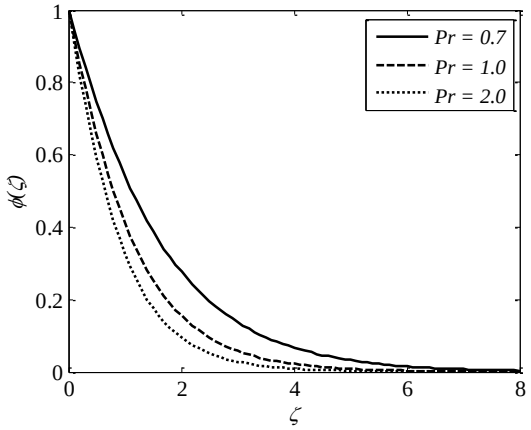

Fig. 17. Impact of $\Pr$ on $\phi(\zeta)$

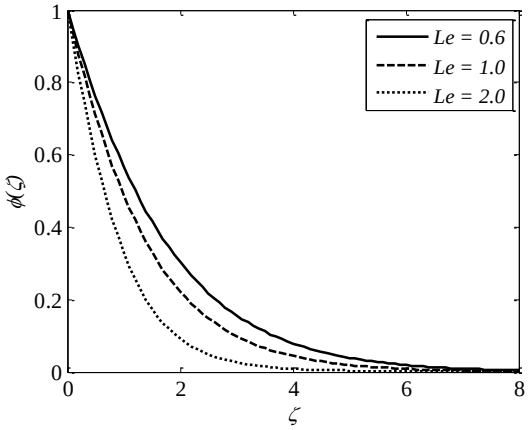

Fig. 18. Impact of Le on $\phi(\zeta)$

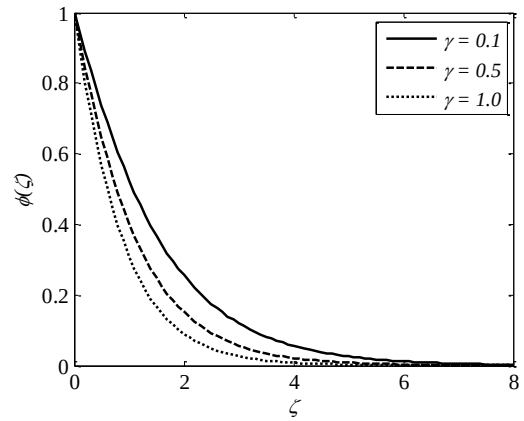

Fig. 19. Impact of γ on $\phi(\zeta)$

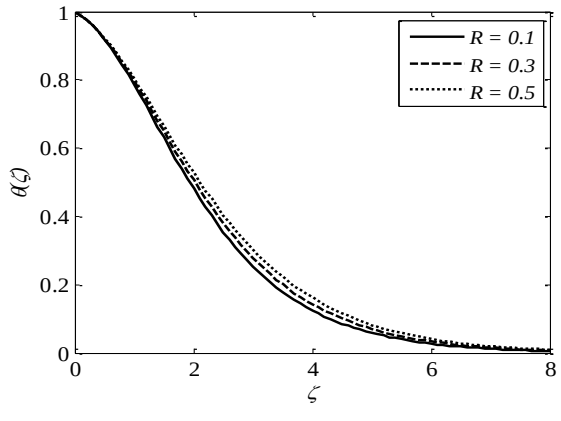

Fig. 20. Impact of R on $\theta(\zeta)$

From Figures 21 to 23, it is clear that an increase in the inclination angle Ω diminishes the skin friction coefficient and but has the opposite impact on the Nusselt and Sherwood numbers. Opposite trend is observed with M .

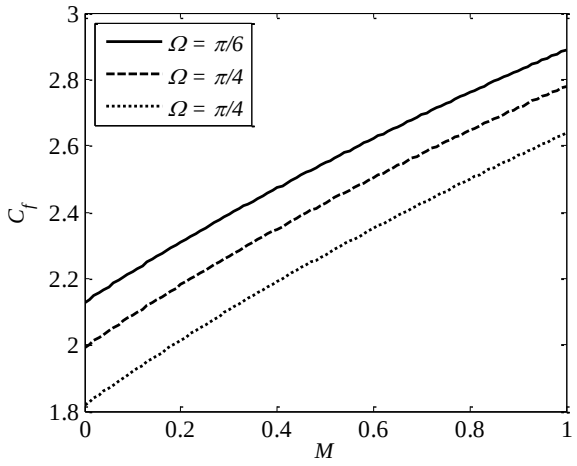

Fig. 21. Impact of Ω and M on C_f

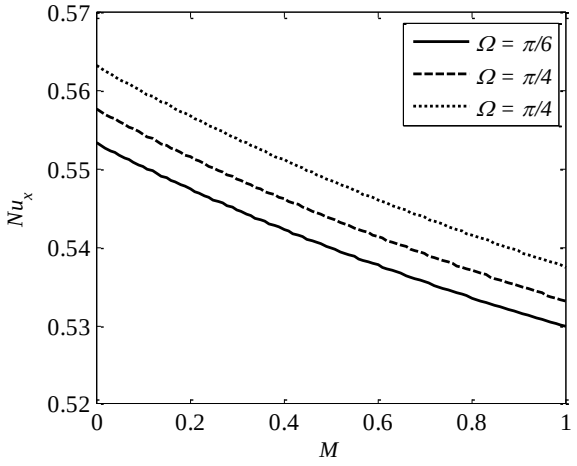

Fig. 22. Impact of Ω and M on Nu_x

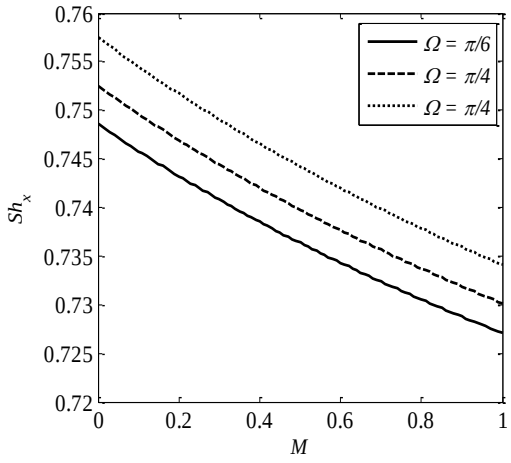

Fig. 23. Impact of Ω and M on Sh_x

4. Conclusions

This study explored the combined effects of heat and mass transfer on Casson nanofluid flow over a non-linear inclined stretching sheet. Also discussed is the impact of heat generation/absorption and chemical reaction under the influence of the Soret and Dufour effects. The effects of adjusting various parameters are very much on purpose. The following are the significant conclusions drawn from the present investigation:

I. When the values of magnetic field parameter is increased, the resulting effect is a reduction in velocity.
II. The temperature rises as the Brownian motion parameter is allowed to rise to higher levels.
III. It has been observed that an increase in the Dufour constraint values results in an increase in the temperature fields.
IV. When the Casson fluid factor is increased, the velocity distribution becomes more uniform.
V. The skin friction coefficient is reduced by an increase in the inclination parameter, which has the opposite effect on the Nusselt and Sherwood numbers.
VI. The fluid flow distribution can be improved by increasing the values of both the buoyancy and the solutal buoyancy.

Acknowledgements

We appreciate the reviewers' spending the time and making the effort to read the manuscript. We sincerely thank you for your insightful comments and recommendations, which allowed us to increase the manuscript's quality.

References

[1] Choi, S. US, and Jeffrey A. Eastman. *Enhancing thermal conductivity of fluids with nanoparticles*. No. ANL/MSD/CP-84938; CONF-951135-29. Argonne National Lab.(ANL), Argonne, IL (United States), 1995.

[2] Buongiorno, Jacopo. "Convective transport in nanofluids." (2006): 240-250. https://doi.org/10.1115/1.2150834

[3] Eastman, Jeffrey A., S. U. S. Choi, Sheng Li, W. Yu, and L. J. Thompson. "Anomalously increased effective thermal conductivities of ethylene glycol-based nanofluids containing copper nanoparticles." *Applied physics letters* 78, no. 6 (2001): 718-720. https://doi.org/10.1063/1.1341218

[4] Qasim, M., Z. H. Khan, R. J. Lopez, and W. A. Khan. "Heat and mass transfer in nanofluid thin film over an unsteady stretching sheet using Buongiorno's model." *The European Physical Journal Plus* 131 (2016): 1-11. https://doi.org/10.1140/epjp/i2016-16016-8

[5] Andersson, H. I., J. B. Aarseth, N. Braud, and B. S. Dandapat. "Flow of a power-law fluid film on an unsteady stretching surface." *Journal of Non-Newtonian Fluid Mechanics* 62, no. 1 (1996): 1-8. https://doi.org/10.1016/0377-0257(95)01392-X

[6] Khan, W. A., and I. Pop. "Boundary-layer flow of a nanofluid past a stretching sheet." *International journal of heat and mass transfer* 53, no. 11-12 (2010): 2477-2483. https://doi.org/10.1016/j.ijheatmasstransfer.2010.01.032

[7] Yu, Wenhua, David M. France, Jules L. Routbort, and Stephen US Choi. "Review and comparison of nanofluid thermal conductivity and heat transfer enhancements." *Heat transfer engineering* 29, no. 5 (2008): 432-460. https://doi.org/10.1080/01457630701850851

[8] Kakaç, Sadik, and Anchasa Pramuanjaroenkij. "Review of convective heat transfer enhancement with nanofluids." *International journal of heat and mass transfer* 52, no. 13-14 (2009): 3187-3196. https://doi.org/10.1016/j.ijheatmasstransfer.2009.02.006

[9] Godson, Lazarus, B. Raja, D. Mohan Lal, and S. E. A. Wongwises. "Enhancement of heat transfer using nanofluids—an overview." *Renewable and sustainable energy reviews* 14, no. 2 (2010): 629-641. https://doi.org/10.1016/j.rser.2009.10.004

[10] Dash, R. K., K. N. Mehta, and G. Jayaraman. "Casson fluid flow in a pipe filled with a homogeneous porous medium." *International Journal of Engineering Science* 34, no. 10 (1996): 1145-1156. https://doi.org/10.1016/0020-7225(96)00012-2

[11] Ali, Mujeeb, G. Aruna, and R. Srinivasa Raju. "MHD boundary layer casson fluid flow over a vertically inclined plate: grid study and convergence analysis of finite element technique." *Journal of Nanofluids* 7, no. 6 (2018): 1195-1207. https://doi.org/10.1166/jon.2018.1541

[12] Manideep, P., R. Srinivasa Raju, T. Siva Nageswar Rao, and G. Jithender Reddy. "Unsteady MHD free convection flow of casson fluid over an inclined vertical plate embedded in a porous media." In *AIP Conference Proceedings*, vol. 1953, no. 1, p. 140038. AIP Publishing LLC, 2018. https://doi.org/10.1063/1.5033213

[13] Shamshuddin, M. D., S. R. Mishra, and Thirupathi Thumma. "Chemically reacting radiative Casson fluid over an inclined porous plate: a numerical study." In *Numerical Heat Transfer and Fluid Flow: Select Proceedings of NHTFF 2018*, pp. 469-479. Singapore: Springer Singapore, 2018. https://doi.org/10.1007/978-981-13-1903-7_54

[14] Vijayaragavan, R., and M. Angeline Kavitha. "Heat and Mass Transfer in Unsteady MHD Casson Fluid Flow past an Inclined Plate with Thermal Radiation and Heat source/sink." *Research Journal of Engineering and Technology* 9, no. 2 (2018): 214-223. https://doi.org/10.5958/2321-581X.2018.00030.2

[15] Prasad, DVV Krishna, GS Krishna Chaitanya, and R. Srinivasa Raju. "Role of casson fluid on MHD natural convective flow towards vertically inclined plate with hall current." In *AIP Conference Proceedings*, vol. 1953, no. 1, p. 140073. AIP Publishing LLC, 2018. https://doi.org/10.1063/1.5033248

[16] Jain, Shalini, and Amit Parmar. "Multiple slip effects on inclined MHD Casson fluid flow over a permeable stretching surface and a melting surface." *International Journal of Heat and Technology* 36, no. 2 (2018): 585-594. https://doi.org/10.18280/ijht.360222

[17] Sailaja, S. V., B. Shanker, and R. Srinivasa Raju. "Finite element analysis of magneto-hydrodynamic casson fluid flow past a vertical plate with the impact of angle of inclination." *Journal of Nanofluids* 7, no. 2 (2018): 383-395. https://doi.org/10.1166/jon.2018.1456

[18] Rawi, N. A., M. R. Ilias, Y. J. Lim, Z. M. Isa, and S. Shafie. "Unsteady mixed convection flow of Casson fluid past an inclined stretching sheet in the presence of nanoparticles." In *Journal of Physics: Conference Series*, vol. 890, no. 1, p. 012048. IOP Publishing, 2017. https://doi.org/10.1088/1742-6596/890/1/012048

[19] Raju, R. Srinivasa, B. Mahesh Reddy, and G. Jithender Reddy. "Finite element solutions of free convective Casson fluid flow past a vertically inclined plate submitted in magnetic field in presence of heat and mass transfer." *International Journal for Computational Methods in Engineering Science and Mechanics* 18, no. 4-5 (2017): 250-265. https://doi.org/10.1080/15502287.2017.1339139

[20] Rashidi, Mohammad M., Zhigang Yang, Muhammad M. Bhatti, and Munawwar Ali Abbas. "Heat and mass transfer analysis on MHD blood flow of Casson fluid model due to peristaltic wave." *Thermal Science* 22, no. 6 Part A (2018): 2439-2448. https://doi.org/10.2298/TSCI160102287R

[21] Abbas, M. Ali, Y. Q. Bai, M. M. Rashidi, and M. M. Bhatti. "Application of drug delivery in magnetohydrodynamics peristaltic blood flow of nanofluid in a non-uniform channel." *Journal of Mechanics in Medicine and Biology* 16, no. 04 (2016): 1650052. https://doi.org/10.1142/S0219519416500524

[22] Vishalakshi, Angadi Basettappa, Thippaiah Maranna, Ulavathi Shettar Mahabaleshwar, and David Laroze. "An effect of MHD on non-Newtonian fluid flow over a porous stretching/shrinking sheet with heat transfer." *Applied Sciences* 12, no. 10 (2022): 4937. https://doi.org/10.3390/app12104937

[23] Maranna, T., K. N. Sneha, U. S. Mahabaleshwar, Ioannis E. Sarris, and Theodoros E. Karakasidis. "An effect of radiation and MHD Newtonian fluid over a stretching/shrinking sheet with CNTs and mass transpiration." *Applied Sciences* 12, no. 11 (2022): 5466. https://doi.org/10.3390/app12115466

[24] Mahabaleshwar, Ulavathi Shettar, Thippaiah Maranna, and Filippos Sofos. "Analytical investigation of an incompressible viscous laminar Casson fluid flow past a stretching/shrinking sheet." *Scientific Reports* 12, no. 1 (2022): 18404. https://doi.org/10.1038/s41598-022-23295-6

[25] Maranna, Thippaiah, Ulavathi S. Mahabaleshwar, and Michael I. Kopp. "The Impact of Marangoni Convection and Radiation on Flow of Ternary Nanofluid in a Porous Medium with Mass Transpiration." *Journal of Applied and Computational Mechanics* 9, no. 2 (2023): 487-497.

[26] Maranna, T., K. N. Sneha, U. S. Mahabaleshwar, and Basma Souayeh. "An impact of heat and mass transpiration on magnetohydrodynamic viscoelastic fluid past a permeable stretching/shrinking sheet." *Heat Transfer*.

[27] Mahesh, R., U. S. Mahabaleshwar, Emad H. Aly, and Oronzio Manca. "An impact of CNTs on an MHD Casson Marangoni boundary layer flow over a porous medium with suction/injection and thermal radiation." *International Communications in Heat and Mass Transfer* 141 (2023): 106561. https://doi.org/10.1016/j.icheatmasstransfer.2022.106561

[28] Mahabaleshwar, U. S., Emad H. Aly, and T. Anusha. "MHD slip flow of a Casson hybrid nanofluid over a stretching/shrinking sheet with thermal radiation." *Chinese Journal of Physics* 80 (2022): 74-106. https://doi.org/10.1016/j.cjph.2022.06.008

[29] Singh, Jitender, A. B. Vishalakshi, U. S. Mahabaleshwar, and Gabriella Bognar. "MHD Casson fluid flow with Navier's and second order slip due to a perforated stretching or shrinking sheet." *Plos one* 17, no. 11 (2022): e0276870. https://doi.org/10.1371/journal.pone.0276870

[30] Kay, E. D., Stephen Hibberd, and Henry Power. "A multi-layer integral model for locally-heated thin film flow." *Journal of Computational Physics* 336 (2017): 51-68. https://doi.org/10.1016/j.jcp.2017.01.066

[31] Alharbi, Abdulghani, and Shailesh Naire. "An adaptive moving mesh method for thin film flow equations with surface tension." *Journal of Computational and Applied Mathematics* 319 (2017): 365-384. https://doi.org/10.1016/j.cam.2017.01.019

[32] Shuaib, N. H., Henry Power, and S. Hibberd. "BEM solution of thin film flows on an inclined plane with a bottom outlet." *Engineering analysis with boundary elements* 33, no. 3 (2009): 388-398. https://doi.org/10.1016/j.enganabound.2008.06.007

[33] Yu, Y. Q., and X. Cheng. "Experimental study of water film flow on large vertical and inclined flat plate." *Progress in Nuclear Energy* 77 (2014): 176-186. https://doi.org/10.1016/j.pnucene.2014.07.001

[34] Rafique, Khuram, Muhammad Imran Anwar, Masnita Misiran, Ilyas Khan, S. O. Alharbi, Phatiphat Thounthong, and K. S. Nisar. "Numerical solution of casson nanofluid flow over a non-linear inclined surface with soret and dufour effects by keller-box method." *Frontiers in Physics* 7 (2019): 139. https://doi.org/10.3389/fphy.2019.00139

[35] Sunitha, Cheela, Prathi Vijaya Kumar, Giulio Lorenzini, and Shaik Mohammed Ibrahim. "A Study of Thermally Radiant Williamson Nanofluid Over an Exponentially Elongating Sheet with Chemical Reaction Via Homotopy Analysis Method." *CFD Letters* 14, no. 5 (2022): 68-86. https://doi.org/10.37934/cfdl.14.5.6886

[36] Reddy, Thummala Sankar, P. Roja, S. Mohammed Ibrahim, Giulio Lorenzini, and Nor Azwadi Che Sidik. "Characteristic of Thermal Radiation on MHD Fluid Stream of Nano-Fluid over an Exponentially Elongating Sheet by Means of Warm and Mass Fluxes." *CFD Letters* 14, no. 4 (2022): 80-90. https://doi.org/10.37934/cfdl.14.4.8090

[37] Roja, P., T. Sankar Reddy, S. M. Ibrahim, Giulio Lorenzini, and Nor Azwadi Che Sidik. "The Effect of Thermophoresis on MHD Stream of a Micropolar Liquid Through a Porous Medium with Variable Heat and Mass Flux and Thermal Radiation." *CFD Letters* 14, no. 4 (2022): 118-136. https://doi.org/10.37934/cfdl.14.4.118136

[38] Alao, F. I., A. I. Fagbade, and B. O. Falodun. "Effects of thermal radiation, Soret and Dufour on an unsteady heat and mass transfer flow of a chemically reacting fluid past a semi-infinite vertical plate with viscous dissipation." *Journal of the Nigerian mathematical Society* 35, no. 1 (2016): 142-158. https://doi.org/10.1016/j.jnnms.2016.01.002

[39] Omowaye, A. J., A. I. Fagbade, and A. O. Ajayi. "Dufour and soret effects on steady MHD convective flow of a fluid in a porous medium with temperature dependent viscosity: Homotopy analysis approach." *Journal of the Nigerian Mathematical Society* 34, no. 3 (2015): 343-360. https://doi.org/10.1016/j.jnnms.2015.08.001

[40] Amanulla, C. H., S. Saleem, Abderrahim Wakif, and M. M. AlQarni. "MHD Prandtl fluid flow past an isothermal permeable sphere with slip effects." *Case Studies in Thermal Engineering* 14 (2019): 100447. https://doi.org/10.1016/j.csite.2019.100447

[41] Ahmed, Sameh E., and Z. Z. Rashed. "MHD natural convection in a heat generating porous medium-filled wavy enclosures using Buongiorno's nanofluid model." *Case Studies in Thermal Engineering* 14 (2019): 100430. https://doi.org/10.1016/j.csite.2019.100430